MODELING AND ASSESSMENT OF INTEGRAL CRACK ARREST ZONES IN CFRP LAMINATES

Matthew A. Dilligan, Keith T. Kedward
University of California, Santa Barbara

Keywords: *Fracture, Crack Arrest, Buffer Strips, Modeling*

Abstract

A methodology for the analysis of crack arrest in buffer-strip-equipped fiber-reinforced composite structures is presented based on the large scale sliding of bridging lamina. Using a numeric implementation of the proposed model, simulations are conducted to calculate the resultant crack tip stress intensity factor for a range of crack configurations and loading levels in a quasi-isotropic carbon/epoxy laminate with integral glass/epoxy buffer strips. Results are compared to available experimental data to assess the initial model results, and are analysed to identify potential drivers for buffer strip sizing and optimisation. Areas for improvement within the model implementation are discussed, and future experimental work to validate and calibrate the model is presented.

1 Introduction

Understanding the growth and arrest of cracks in composite materials is critical for their effective utilization in fatigue-sensitive applications such as primary aircraft structures. As design standards for these structures advance beyond the conservative no-crack-growth requirement, design concepts for the arrest of cracks become extremely valuable, particularly if they can be incorporated with a minimal weight and production penalty. Arrest components are even more important for applications where significant damage is possible during routine use, such as military vehicles subject to hostile fire and harsh operating conditions.

Recent industry work has focused on methods to more efficiently produce composite aircraft structures, including the utilization of a standard, pre-fabricated laminate stack. The manufacturing method for this base material allows a great deal of customization of the laminate composition, including local substitution of alternate fibers into the laminate stack as illustrated in Fig. 1. This has led to interest in the use of this capability to fully integrate crack-arresting buffer strips into the resultant structure with a minimum of consideration (and cost) during layup and processing. These elements utilize a local region of high strain-to-failure fibers such as glass, Zylon or Kevlar to blunt the stress intensity at the tip of a crack growing through the relatively brittle carbon fibers.

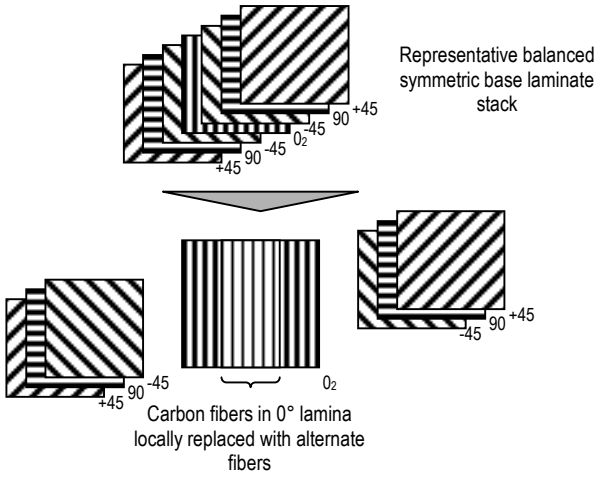

Fig. 1. Local fiber substitution and buffer strip construction

The concept of low-modulus buffer strips is not new, dating back to some of the earliest efforts at creating damage tolerant aerospace structures [1]. Initial efforts focused on the external addition of material to an existing composite structure, while later work integrated the alternate materials directly into the base laminate stack [2]. This work has clearly demonstrated the value of such elements, though the development of an analytic model quantifying the benefit has lagged the demonstration of their value. The goal of this paper is to present a practical model to quantify the effect of a given

buffer strip architecture, to allow for effective design and optimization of crack arrest elements elements.

2 Background

While the failure of composites is complicated by the meso-scale inhomogeneity inherent in such materials, the situation is simplified by the consideration of a complete structural laminate containing a relatively balanced mix of lamina. In these cases, the classic mode I crack tip stress intensity factor has proven a reliable criteria for prediction of self-similar mode I crack growth [3,4,5]. Buffer strips arrest crack growth by introducing a portion of the material that does not fail as the crack progresses through it, and which serves to bridge and provide closure tractions to the crack face as shown in Fig. 2. If successful, the closure tractions reduce the stress intensity at the crack tip to a level below that necessary to extend the crack.

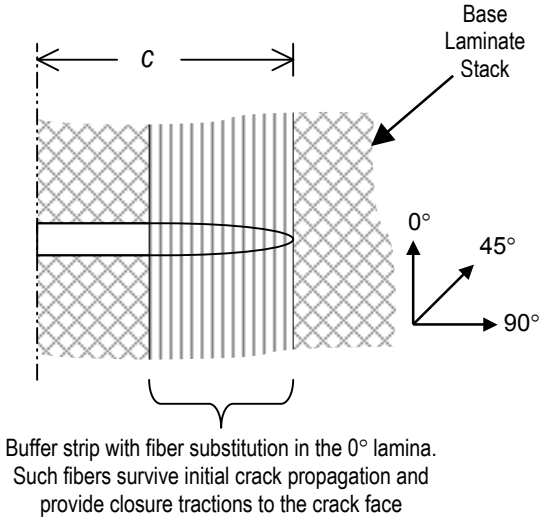

Fig. 2. Basic architecture of the crack-bridging buffer strip

The crack arrest properties of buffer strips, whether external or integrated, result from two mechanism; the decoupling of the bridging buffer material from the base laminate, and the subsequent application of closure stresses across the propagating crack. Without decoupling, the buffer material will fracture as the crack propagates through it, as indeed many of the materials found effective for buffer strips fail at a lower tensile stress than the materials comprising the base laminate. Without closure tractions, no mechanism exists to retard the growth of the crack in the base laminate and resultant failure of the structure; the surviving buffer material having little inherent load carrying capacity. The ideal buffer strip, therefore, will decouple from the base material sufficiently to avoid fracture as the crack propagates into it, but will remain sufficiently linked to the base laminate to provide support to the base material to resist growth of the crack.

Previous work by NASA provides insight into the roles that these mechanisms play in the arrest of cracks. Poe and Kennedy [2] tested a number of integral buffer strips configurations utilizing a range of substitute materials, including using the identical material that comprised the balance of the laminate. In such specimens the buffer strip was defined not by a variation in material but by the inclusion of perforated Mylar strips on either side of the “buffer” fibers. Simply by reducing the interface shear strength and promoting interlaminar decoupling significant crack arrest affects were observed, though to a lesser extent than configurations utilizing higher strain-to-failure materials. Maximum benefit was found with materials with significantly higher strain-to-failures than the base laminate, delaying failure of the buffer materials and providing crack closure tractions even with relatively large crack face displacements.

3 Modeling

3.1 Model Overview

The proposed model takes a mechanistic view of crack propagation, with the goal of determining the external tractions and stresses that drive and retard the propagation of the crack. Once the governing forces are described, the resultant stress intensity factor at the crack tip can be calculated and compared to the equivalent stress intensity for a structure without buffer strips. These methods are similar to those used historically on both homogeneous, isotropic materials as well as specialized composites. As an example of the former, the Dugdale strip yield model [4] recognizes the process zone resulting from localized yielding to provide closure tractions at the virtual crack tip. Work on ceramic and similarly brittle matrix composites [6,7] has used a more micro-mechanical model of fiber/matrix interactions to calculate closure tractions on the crack face and the resultant reduction of crack tip stress intensities.

The ordered meso-scale nature of laminated composites suggests a model close in scale to those developed for brittle matrix composites, though the significantly higher fiber volume fraction makes it unlikely that individual fiber behavior will be decoupled as assumed by the large scale sliding models presented in such [6]. Qualitative

examination of available laminate failure testing [2,3] has demonstrated the dominance of laminate-based behavior during failure, and it is assumed that laminate-scale processes will similarly dominate the behavior within the buffer strip.

The core element of this model is the relationship derived between crack face opening displacement and the resultant stress in bridging fibers within the buffer strip zone. To derive this, a force balance similar to that presented in Marshall et al. [6] is utilizes, though the geometry of such is modified to focus on lamina-scale, rather than fiber-scale, behavior. As shown in Fig. 3, the primary load transfer mechanism between the bridging laminate and the bulk of the laminate is through a shear traction along the disbonded length nearest the crack face, directly analogous to the shear force utilized in the fiber-based derivations. Using basic elasticity relationships, the relationship between the crack face displacement and the resultant stress in the bridging laminate can then be found.

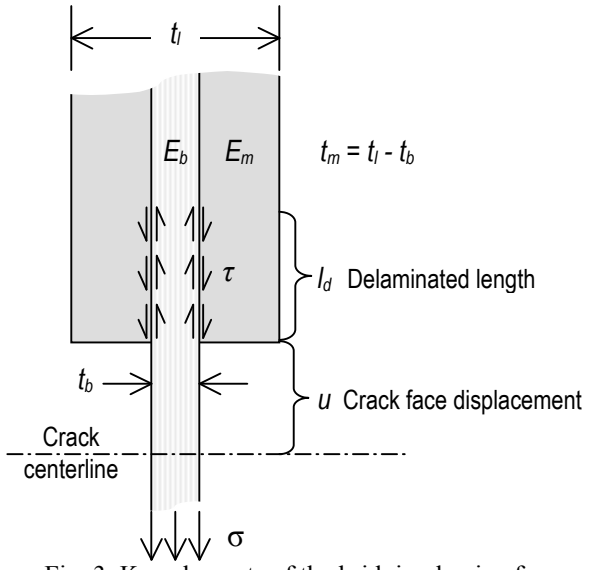

Fig. 3. Key elements of the bridging lamina force balance, side view

Eq.1 and 2 are the governing relationship between crack face displacement and crack closure traction, where E_b, t_b and E_m, t_m are the tensile modulus and thickness of the bridging lamina and the balance of the laminate, respectively. The traction between disbonded lamina is given by τ. An outline of the derivation can be found in the appendix.

$$p[x] = \frac{t_b}{t_l}\sigma = \beta \cdot \left(\frac{t_b}{t_b + t_m}\right)\sqrt{u[x]} \qquad (1)$$

$$\beta = 2 \cdot \sqrt{\frac{\tau \cdot E_b}{t_b} \cdot (1-\eta)}$$
$$\eta = \frac{t_b \cdot E_b}{t_m \cdot E_m} \qquad (2)$$

$$u[X] = \frac{4 \cdot c}{\pi \cdot G_c} \int_X^1 \frac{s}{\sqrt{s^2 - X^2}} \times \left(\int_0^s \frac{p[t] \cdot dt}{\sqrt{s^2 - t^2}} \right) \cdot ds \qquad (3)$$

The crack face displacement is determined by simple superposition of the unbridged crack solution and the crack face tractions from the relationship given by Sneddon and Lowengrub [8] in Eq. 3. Due to the interdependence of these functions they must be solved simultaneously, and due to their complexity a discretized numerical solution is utilized in this study.

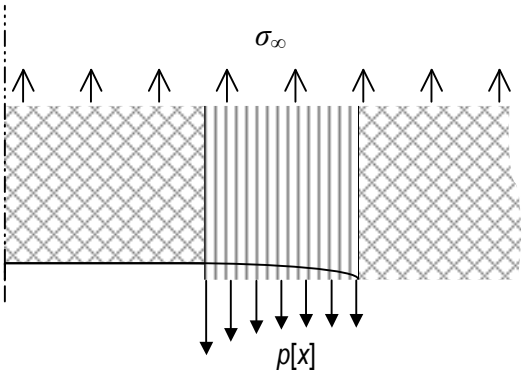

Fig. 4. Tractions in the crack region

Once a self-consistent solution for the bridging stresses has been reached, the complete loading of the crack can be determined, as illustrated in Fig. 4. Stress intensity at the crack tip can then be calculated by superposition of the unbridged crack tip stress intensity in Eq. 4 and the stress intensity resulting from the crack surface tractions, weighted as given in Eq. 5 [9,10].

$$K_I = \sigma_\infty \sqrt{\pi \cdot c} \qquad (4)$$

$$K_I' = 2\sqrt{\frac{c}{\pi}} \cdot \int_0^1 \frac{\sigma_\infty - p[X]}{\sqrt{1 - X^2}} \cdot dX \qquad (5)$$

For the most part, the material properties utilized in these relationships are well established and easily derived from standard material testing. The exception to this is τ, the shear traction between adjacent decoupled lamina, assumed in this model to be constant over the surface of the interface. As this

is a key driver of both bridging lamina decoupling and crack surface traction, the poor definition of such is a weakness of the current model. Future experimental work as described later is planned to investigate this mechanism and define this property more effectively.

In the absence of a well-characterized interface between disbonded lamina, the affect of this variable becomes an avenue for both investigation and potential optimization of the crack arrest element. Previous work has clearly demonstrated the sensitivity of crack-arrest mechanisms to the degree of interlaminar decohesion, with the optimal interface allowing decoupling of the bridging fibers from the base laminate to prevent fracture while retaining sufficient cohesion to exert significant closure stresses on the advancing crack. Given the high degree of tailoring possible through material selection, chemical treatment (fiber sizing and treatment), and mechanical modification (the perforated Mylar strips utilized by Poe et al. [2]), it is likely that this material property will constitute a key design variable for such crack arrest elements.

3.2 Material Properties and Isotropy

The function utilized for crack surface displacement is rooted in the classic model of linear isotropic solid mechanics. The actual configuration under consideration clearly differs from this idealization in two aspects: uniformity and isotropy.

The former is violated by the presence of the buffer strip, whose elastic properties differ from those in the base laminate surrounding it. Violation of this assumption is negated, however, if the crack tip is positioned within the buffer strip zone. When this condition is satisfied, the crack face displacement for the laminate region containing bridging fibers, and as a result the crack face tractions, are determined solely by the material properties within a single material zone. Results of both the simulations below, as well as the available experimental work [1,2], suggest that the crack states representing maximum crack growth arrest satisfy this condition. Given this, the current implementation of the model utilizes only the buffer zone material properties, and calculated stress intensity factors for cracks extending beyond the buffer zone are expected to contain a minor degree of error not yet quantified.

The latter assumption of isotropy is almost always violated in the buffer strip zone, though it may be satisfied on a macroscopic scale within the base laminate if a quasi-isotropic layup is under consideration. At this time, no anisotropic crack solutions have been attempted to allow for rigorous consideration of this affect. The net affect of material anisotropy on calculated stress intensity is limited, however, by the nature of the crack face displacement, which is primarily a function of in-plane shear deformation of the material. As a result, the affect of material anisotropy on crack face displacements, and as a result crack face tractions and crack tip stress intensity, should be minimal.

3.2 Implementation

The primary equations of the crack bridging model were implemented in C++ using a numerical integration scheme to solve both crack face displacement and crack tip stress intensity. Due to the sensitivity of the K_I calculation to forces at the crack tip, a logarithmic scale was utilized to heavily bias the fineness of integration to the region of the crack tip.

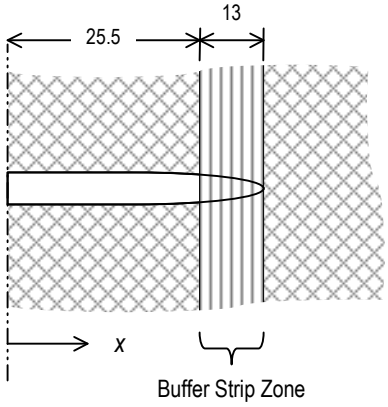

Fig. 5. Simulation buffer strip dimensions [mm]

Initial modeling efforts utilize the material characterizations provided in Soden et al. [11], and focused on the analysis of a quasi-isotropic CFRP laminate with layup $[45/90/-45/0]_s$, with the buffer strip defined by the substitution of GRP in the 0° lamina at the center of the laminate. To allow comparison with the most comprehensive work to date, materials and geometry for simulations were modeled closely on the work of Poe et al. [2] as illustrated in Fig. 5.

It should be noted that due to the preliminary nature of the proposed model, limited effort was focused on optimization of the numeric methods, though such work is planned should preliminary results warrant.

3.3 Simulation Program

Three major sets of simulations were performed using the model described above. The first set of simulations investigated the affect of the poorly characterized interlaminar shear traction utilizing the presumed existence of a crack extending through but not beyond the buffer strip as illustrated in Fig. 5. For this configuration, the resultant stress intensity factor at the crack tip under a constant far field stress of σ_∞ = 200MPa is calculated for a range of disbonded interface shear values. It is reasonable to expect that the interface shear will be on the order of but less than the shear strength of the matrix S_m, therefore interface shear values were scaled as a percentage of this value. Ten simulations were initially conducted with an interface shear range of 10-100% S_m, with additional simulations carried out in the vicinity of significant behavioral shifts.

The second set of simulations seeks to identify the point of maximum arrest for a crack impinging on and passing through a buffer strip crack arrest zone. These simulations assume the existence of a crack entering and passing through the buffer zone at a constant far field stress of σ_∞ = 200MPa, again calculating the resultant stress intensity factor at the crack tip. Utilizing the results of the previous set of simulations, a constant interlaminar shear value of $\tau = 0.3*S_m$ is used for all crack configurations.

The third set of simulations investigates the progressive loading of a fixed crack geometry. The maximum crack arrest configuration identified above is subjected to an increasing far field stress and resultant crack tip stress intensity is calculated. Again, a constant interlaminar shear traction of $\tau = 0.3*S_m$ is utilized for these models.

4. Model Results

4.1 Overview

Initial results from the model appear quite reasonable, with resultant crack face displacements smooth and without discontinuities. Fig. 6 illustrates the calculated crack face displacement for an unbridged crack and one with a bridging buffer strip. As expected, significant crack closure is apparent in the region of the buffer strip, while displacements outside the zone appear to quickly revert to the unbridged solution and increases $\sim r^{-1/2}$.

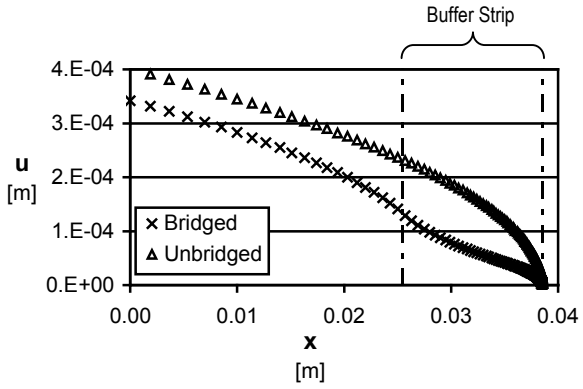

Fig. 6. Crack face displacement for an unbridged and bridged crack with for $\tau = 0.3*S_m$ and σ_∞ = 200 MPa

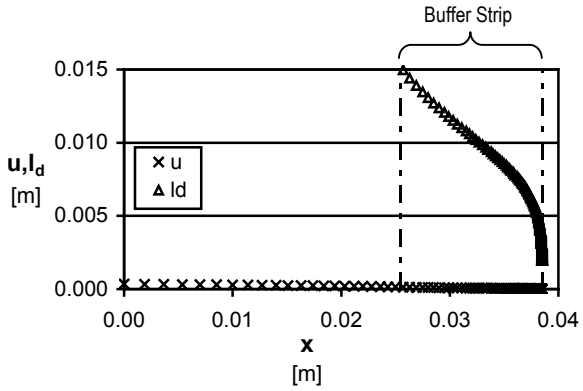

Fig. 7. Crack face displacement and delamination zone at the crack tip for $\tau = 0.3*S_m$ and σ_∞ = 200 MPa

A key driver of the crack arrest affect is the decoupling of the bridging fibers from the base laminate. A simple force balance allows determination of disbanded length l_d from closure traction $p[x]$ and material properties as provided in Eq. 6.

$$l_d[x] = \left(\frac{t_b + t_m}{2 \cdot \tau} \right) \cdot p[x] \qquad (6)$$

Utilizing this relationship, the size of the delamination zone in the region of the buffer strip can be calculated, and is illustrated in Fig. 7, superimposed over the crack opening displacement for a representative set of results. In the case shown, delamination is greatest further from the crack tip with a magnitude of l_d = 15mm, essentially equal to the maximum possible delamination length as limited by bridging fiber strength. Further loading of the crack, or an increase in the interlaminar shear, would result in the onset of bridging fiber failure and a loss of arrest capacity.

4.2 Interface Shear Progression

Modification of the interlaminar shear traction between the bridging fibers and the base matrix shows a pattern very much in line with what would reasonable be expected. As the interface traction increases, the stress in the bridging fibers similarly increases resulting in crack closure and a decrease in the net stress intensity at the crack tip as illustrated in Fig. 8.

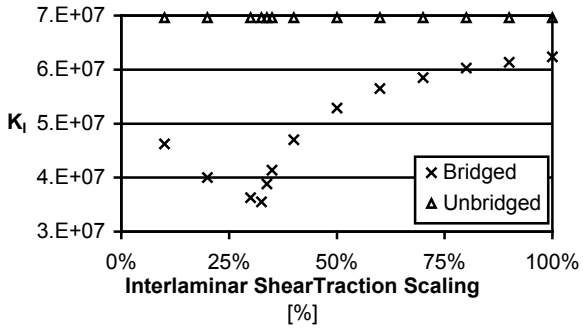

Fig. 8. Stress concentration variation with scaling of interlaminar shear traction with σ_∞ = 200 MPa

The upper limit of this increase in crack bridging occurs as stress in the fibers furthest away from the crack tip (and hence with the greatest crack face opening) exceeds the tensile strength of such fibers, at which those fibers are no longer able to contribute bridging and crack closure tractions. For the simulations performed, fiber failure first occurred at an interface shear value above 33% matrix shear strength ($\tau = 0.33*S_m$).

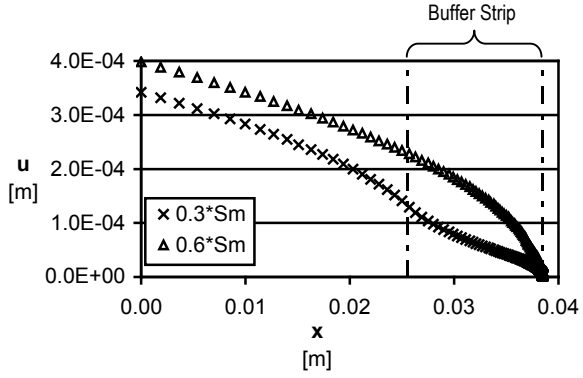

Fig. 9. Crack face displacements pre- and post- bridging fiber failure initiation, illustrated with the cases of $\tau = 0.3*S_m$ and $\tau = 0.6*S_m$, with σ_∞ = 200 MPa

Once fiber fracture has begun there is a rapid drop-off of crack arrest capacity. Measured by the magnitude of stress intensity reduction, the crack closure effect with $\tau = 0.6*S_m$ is less than half the maximum closure affect achieved at $\tau = 0.3*S_m$. At $\tau = 0.6*S_m$, only 13% of the width of the bridging section remains intact and the net stress intensity factor is 81% of the unbridged value. Fig. 9 compares the resultant crack face displacements for an interlaminar shear value of 30% and 60% of the matrix shear strength ($\tau = 0.3*S_m$, $\tau = 0.6*S_m$)

4.3 Crack Length Progression

Based on the results of the interface shear progression analysis, further analyses utilize an interface shear traction of 30% of the matrix shear strength ($\tau = 0.3*S_m$). Using this value, the second set of progressive simulations investigated the degree of closure and arrest on a crack progressing into and through the buffer strip zone at a constant far-field stress.

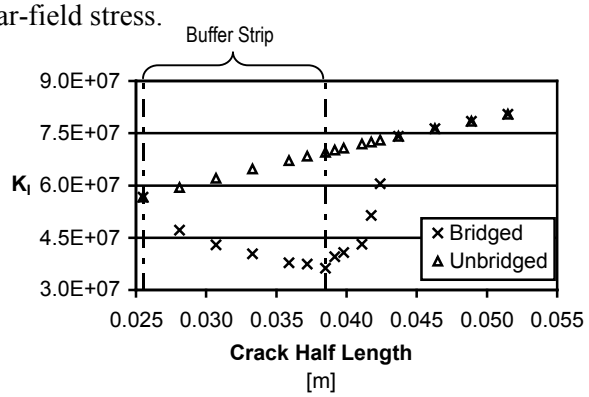

Fig. 10. Stress concentration variation with progression of crack through the buffer strip with $\tau = 0.3*S_m$ and σ_∞ = 200 MPa

As shown in Fig. 10, net stress intensity at the crack tip went down as the crack penetrated further into the arrest zone, even with the growth in base stress intensity due to the increasing half length of the crack. Stress intensity was minimized at the point the crack tip had reached the far side of the buffer zone but had not penetrated the base laminate beyond. Once the crack tip had penetrated beyond the buffer strip, crack closure and arrest affects were still observed, though to a lesser magnitude than at the point described above. Significant benefits were observed until the point at which bridging fiber failure initiated, at which point the crack quickly reverted to an unbridged condition.

It should be noted that the fracture of the arrest fibers occurs very suddenly, in a cleavage-type process; the failure of a subset of the fibers transferring sufficient load to the remaining fibers to lead to their subsequent failure except for in a very small range of openings. Such a sudden final failure closely matches the experimental results to date [2].

4.4 Far Field Stress Progression

Results from the third and final set of simulations provided insight into the progressive loading of a fixed crack configuration. As shown in Eq. 4, the crack tip stress intensity factor for an unbridged crack will increase linearly with the increase in far field stress. The stress intensity at the bridged crack tip will increase as well, but at a lower rate than the unbridged crack. The magnitude of the stress intensity reduction is greatest just prior to the initiation of bridging fiber failure as shown in Fig. 11. In the case of the given crack configuration this occurs at a far field stress above ~210MPa.

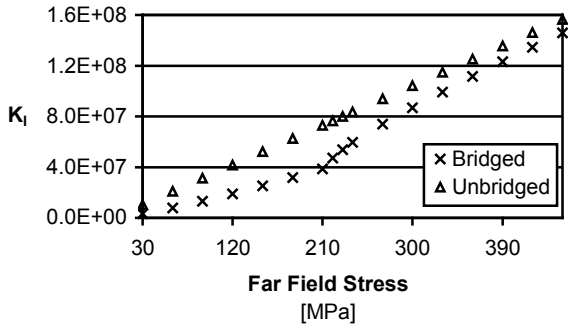

Fig. 11. Stress concentration variation with increasing far field stress with $\tau = 0.3*S_m$

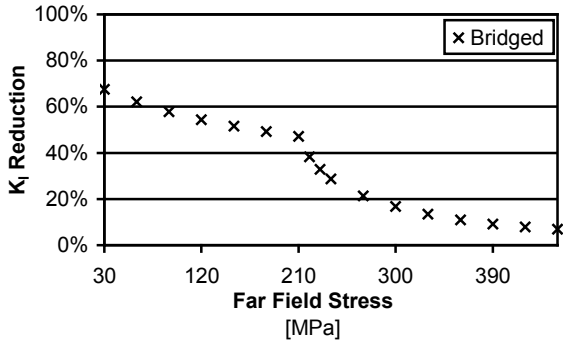

Fig. 12. Percentage stress concentration reduction with increasing far field stress with $\tau = 0.3*S_m$

Crack bridging and arrest is still observed once fiber fracture begins, though the effectiveness of such drops off quickly as the field stress intensity increases. Fig. 12 shows the percentage reduction in crack tip stress intensity due to the bridging of the buffer strip, with a clear shift once bridging fiber failure begins above σ_∞ = 210 MPa. It should be noted that due to the constrained position of the crack tip within the buffer strip, full failure of all bridging fibers will never occur. Instead, the point of fiber failure will asymptotically approach the crack tip, as partially illustrated in the plot of fiber stresses for multiple far field stresses in Fig. 13.

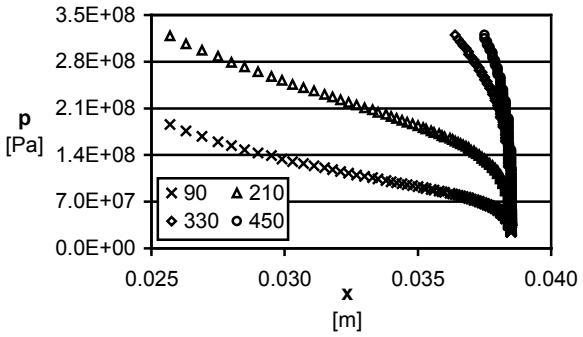

Fig. 13. Bridging fiber stress within the buffer strip with $\tau = 0.3*S_m$ for σ_∞ = 90, 210, 330, and 450 MPa

5 Discussion

5.1 Model validation

Though results for directly comparable experiments were not available in time for this conference, the output of the model correlates very well on a qualitative basis to previous work in the area.

As discussed before and demonstrated in the simulations, the model is highly sensitive to the interlaminar behavior and the resulting traction between disbonded lamina. This is very much in line with the findings of Poe and Kennedy [2], who were able to demonstrate crack arrest properties without material substitution by simply weakening the interface between a localized set of transverse fibers and the surrounding laminate. Additional visualization work carried out in that study confirmed the presence of large scale delamination between the crack-bridging fibers and the fracturing laminate, though no attempt was made to correlate its progression with increasing loading.

The damage progression and failure mode implied by the model also corresponds with available experimental results. As demonstrated in numerous previous efforts [1,2], crack progression behaves essentially as it would in a uniform panel until the crack reaches the buffer strip; at which point it is arrested. Large-scale delamination then progresses between the bridging fibers of the buffer strip and the surrounding laminate, but the crack does not progress beyond the buffer strip until final failure is reached in a quick, cleavage-type failure.

As illustrated in Fig. 10, the minimum crack tip stress intensity is reached at the point where the crack has penetrated the width of the buffer strip but

not beyond. As loading increases, the bridging fiber load increases with a resultant increase in the magnitude of stress concentration reduction, as illustrated in Fig. 12. Once the crack tip stress intensity reaches a level sufficient to cause crack progression beyond the buffer strip, the crack is unstable; further progression will result in an increasing stress intensity factor given a constant far field stress as again illustrated in Fig. 10.

5.2 Results and Implications

While few conclusions can be reached from the model results until they are rigorously validated through experimental comparison, observations to date have provided encouraging directional insights into the optimization of buffer strips. The strong sensitivity of crack bridging and stress intensity reduction to interlaminar shear tractions emphasizes the importance of this material property in the design of these elements. Given the high degree of tailoring possible for this property through fiber selection and treatment, it is expected that controlling such will play a major role in the design of these arrest elements. Conclusions beyond this, however, are premature pending experimental validation of the model and the constituent failure processes.

5.3 Future Work

Given the encouraging results presented above, the preliminary application of the large scale sliding model clearly warrants further development and investigation. Two primary avenues exist for this development; refinement of the implementation mechanics and validation through focused experimental work.

Refinement of the implementation will primarily focus on the numerical integration schemes utilized, specifically to address the presence of singularity-type terms in both the crack opening (Eq. 3) and stress concentration (Eq. 5) integrations. The use of more advanced discretization schemes and alternate coordinate systems is also being investigated, again to increase computational fidelity in these regions.

Work is also underway to conduct a focused experimental program to validate and refine the proposed bridging model. Experiments in this program will include both fully-characterized fracture testing of buffer strip components as well as specialized testing to characterize the processes involved in bridging laminate decoupling. Based on the results of these experiments, the constant-shear-traction based bridging model will be revisited and modified as appropriate, potentially through incorporation of a shear-lag type analysis.

Basic testing of buffer strip specimens will utilize progressive far-field strain loading to determine far-field crack growth stress through a buffer strip zone to failure. Secondary data collected will come primarily in the form of visualization and non-destructive examination of samples during the failure process. The goal of this examination is the identification and qualitative characterization of damage processes present during crack growth and arrest.

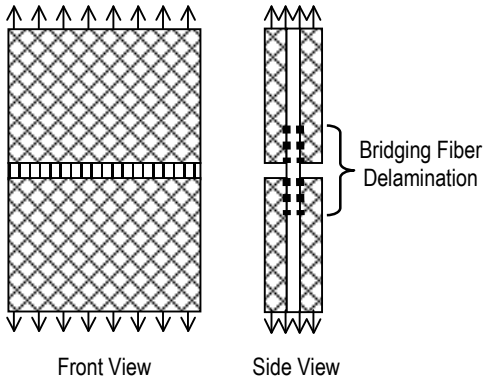

Fig. 14. Test configuration for investigation of bridging fiber delamination

Additional testing will be conducted to accurately characterize and quantify the interaction between the bridging lamina and the surrounding lamina, as this is a weakness in current material data. Fig. 14 illustrates one proposed specimen configuration designed to isolate the material behavior present in the buffer strip zone. Visualization and non-destructive examination should be able to assess the degree of delamination as a function of bridging fiber stress, as well as plotting the relationship between crack face displacement u and bridging fiber stress p. Such work will allow a calculation the interlaminar traction τ as well as a broader assessment of the current model for crack bridging tractions.

References

[1] Huang S.L. and Hess T.E., "A Hybrid Composite Fuselage Design With Integral Crack Arresters". NASA TM X-3377, *3rd Conference on Fibrous Composites in Flight Vehicle Designs*, 1975

[2] Poe C. C. Jr. and Kennedy J. M., "An assessment of buffer strips for improving damage tolerance of composite laminates". *Journal of Composite Materi*als Supplement, Vol. 14, pp 57-70, 1980

[3] Marissen R., Westphal T. and Sterk J.C., "Fracture of quasi-isotropic composite sheets with sharp notches". *Composites Science and Technology*, Vol. 66, Issues 11-12, pp 1803-1812, 2006

[4] Anderson T.L., "*Fracture Mechanics Fundamentals and Applications*". 1st edition, CRC Press, Inc., pp 380-392, 1991

[5] Bao C. and Suo Z., "Remarks on crack bridging concepts". *Appl. Mech. Rev.*, Vol. 45, No. 8, pp 355-366, 1992

[6] Marshall D.B., Cox B.N. and Evans A.G., "The mechanics of matrix cracking in brittle-matrix fiber composites". *Acta Metall.*, Vol. 33, No. 11, pp 2013-2021, 1985

[7] Budiansky B., Hutchinson J.W. and Evans A.G., "Matrix fracture in fiber-reinforced ceramics". *J. Mech. Phys. Solids*, Vol. 34, No. 2, pp 167-189, 1986

[8] Sneddon I. N. and Lowengrub M., "*Crack Problems in the Classical Theory of Elasticity*". 1st edition, Wiley, New York, 1969

[9] Lawn B.R. and Wilshaw T. R., "*Fracture of Brittle Solids*". 2nd edition, Cambridge University Press, 1975

[10] Sih G. C., "*Handbook of Stress Intensity Factors*". 1st edition, Lehigh University, Bethlehem, 1973

[11] Soden P.D., Hinton M.J. and Kaddour A.S., "Lamina properties, lay-up configurations and loading conditions for a range of fibre-reinforced composite laminates". *Composites Science and Technology*, Vol. 58, pp 1011-1022, 1998

Appendix

A-1 Material Properties

The following material properties were used during all simulations described in this paper.

Table A-1. Matrix properties

Material	BSL914C epoxy
E	4.00E+09
G	1.48E+09
v	0.350
Y_t	7.50E+07
Y_c	1.50E+08
S_m	7.00E+07

Source: [11]

E	Elastic modulus	[Pa]
G	In-plane shear modulus	[Pa]
v	Poisson	
Y_t	Tensile strength	[Pa]
Y_c	Compressive strength	[Pa]
S_m	Shear strength	[Pa]

Table A-2. Lamina properties

Material	CFRP	GRP
Fiber	T300	Silenka E-Glass 1200tex
Matrix	BSL914C Epoxy	MY750 / HY917 / DY063 epoxy
vf	0.6	0.6
E_1	1.38E+11	4.56E+10
E_2	1.10E+10	1.62E+10
v_{12}	0.280	0.278
v_{23}	0.400	0.400
G_{12}	5.50E+09	5.83E+09
X_t	1.50E+09	1.28E+09
Y_t	2.70E+07	4.00E+07
S_{12}	8.00E+07	7.30E+07

Source: [11]

vf	Fiber volume fraction	
E_1	Longitudinal modulus	[Pa]
E_2	Transverse modulus	[Pa]
v_{12}	In-plane Poisson	
v_{23}	Out-of-plane Poisson	
G_{12}	In-plane shear modulus	[Pa]
X_t	Longitudinal tensile strength	[Pa]
Y_t	Transverse tensile strength	[Pa]
S_{12}	In-plane shear strength	[Pa]

Table A-3. Laminate Properties

Laminate	Base Laminate	Buffer Strip Laminate	Bridging Lamina	Buffer Strip Minus Bridging Lamina
Layup	$[45/90/-45/0]_s$ CFRP	$[45/90/-45/0]_s$ 0° - GRP bal. - CFRP	$[0]_s$ GRP	$[45/90/-45]_s$ CFRP
E_x	5.41E+10	3.10E+10	4.56E+10	2.62E+10
E_y	5.41E+10	5.16E+10	1.62E+10	5.96E+10
V_{xy}	0.307	0.306	0.278	0.308
G_{xy}	2.07E+10	2.08E+10	5.83E+09	2.58E+10
t	0.002032	0.002032	0.000508	0.001524

Source: [11], SQ5 Lamina property calculation program

E_x	Longitudinal modulus	[Pa]
E_y	Transverse modulus	[Pa]
v_{xy}	In-plane Poisson	
G_{xy}	In-plane shear modulus	[Pa]
t	Laminate thickness	[m]

A-2 Crack Face Traction Equations

The following relationships were utilized to develop the relationship between crack face displacement *u[x]* and crack face traction *p[x]*. Eq. 1a through Eq. 5a are restatements of the relationships utilized in Marshall et al. [6], reformulated for a lamina scale. Eq. 6a relates the

bridging fiber stress σ to the net crack face closure traction $p[x]$.

$$\frac{\sigma_m}{E_m} = \frac{\sigma_b}{E_b} \tag{1a}$$

$$\sigma_m \cdot t_m = 2 \cdot l_d \cdot \tau \tag{2a}$$

$$\sigma \cdot t_b = 2 \cdot l_d \cdot \tau + \sigma_b \cdot t_b \tag{3a}$$

$$\frac{\delta}{l_d} = \frac{l_d \cdot \tau}{t_m \cdot E_m} \tag{4a}$$

$$\frac{\delta + u}{l_d} = \frac{\sigma_b}{E_b} + \frac{l_d \cdot \tau}{t_b \cdot E_b} \tag{5a}$$

$$p[x] = \left(\frac{t_b}{t_b + t_m} \right) \cdot \sigma \tag{6a}$$

E_b, E_m	Elastic modulus of the bridging lamina and the balance of the laminate, respectively	[Pa]
σ_b, σ_m	Stress in the bridging lamina and the balance of the laminate at the point of delamination, respectively	[Pa]
l_d	Delaminated length	[m]
t_b, t_m	Thickness of the bridging and non-bridging lamina, respectively	[m]
τ	Disbonded interlaminar shear traction	[Pa]
σ	Stress in the bridging lamina in the crack opening	[Pa]
δ	Elongation of the non-bridging laminate	[m]
u	Crack face opening displacement	[m]
p	Crack face closure traction	[Pa]